J Supercond Nov Magn (2016) 29:389–400
DOI 10.1007/s10948-015-3270-8

ORIGINAL PAPER

Electrical Properties of Cu Substituted Fe_3O_4 Nanoparticles

Md. Amir[1] · H. Erdemi[2] · M. Geleri[1] · A. Baykal[1]

Received: 20 October 2015 / Accepted: 28 October 2015 / Published online: 7 November 2015

Abstract Diethylene glycol (DEG)-stabilized Cu-substituted Fe_3O_4 nanoparticles ($Cu_xFe_{1-x}Fe_2O_4$, $0.0 \leq x \leq 1.0$) were prepared via polyol method. DEG was used as a stabilizer and dispersant. The X-ray powder diffraction analysis confirmed the formation of cubic spinel structure for all products. The scanning electron microscopy (SEM) micrographs confirmed that all products were roughly spherical in shape with a narrow size distribution and a homogenous shape. The dielectric properties of DEG-stabilized $Cu_xFe_{1-x}Fe_2O_4$ nanoparticles were studied as a function of composition, frequency, and temperature. The dielectric constant (ε'), dielectric loss (ε''), and dielectric loss tangent ($\tan\delta$) indicate different trends with temperature as well as with the composition. The ac and dc conductivities are temperature and frequency dependent. The maximum dc conductivity was found to be about 1.85×10^{-7} S cm^{-1} for $x = 0.0$ at 120 °C. The conduction mechanism is due to electron hopping and temperature-assisted reorganization process.

Keywords Fe_3O_4 · Cu substitution · Polyol method · Dielectric properties · Conductivity

✉ A. Baykal
hbaykal@fatih.edu.tr

[1] Department of Chemistry, Fatih University, 34500 B. Çekmece, Istanbul, Turkey

[2] Department of Polymer Engineering, Yalova University, 77100 Yalova, Turkey

1 Introduction

Magnetite (Fe_3O_4), a fundamental part of spinel ferrite, has been widely used as a recording material, pigment, gas sensor for biomedical treatment, catalyst, electrophotographic developer, and fluxtronic device [1–4]. From few years, Fe_3O_4 composites or transition metals or other noble metals have been studied extensively due their doping with different materials synergetic effect and many potential applications [5–10].

Spinel ferrites MFe_2O_4 (M = divalent metal ion, e.g. Ni, Co, Cu), normally indicated by this formula have been broadly studied by the researchers and scientists since last few decades because of their wide technological applications and promising electromagnetic properties which depend on high electrical resistivity, low eddy current losses, chemical stability and high Curie temperature. The evolution of nanotechnology plays an important role and made the study of these ferrites at nanolevel quite an interesting subject for both fundamental and the application point of view. They have many potential applications in diverse areas due to their strange physical and electrical properties, such as color imaging, information storage, ferrofluids and multi-layer chip inductors, and filters [11–15]. The advantages of the ferrite material are that they yield higher efficiency and have appropriate dielectric loss and low cost hence find larger applications in memory cores and microwave devices [16, 17]. Spinel ferrites' functional properties depend mostly on their real structure's valence state of ions and composition. Generally, ferrites are known by a common formula that is AB_2O_4, where "A" pointed to any cation having 2+ charges such as Cu^{2+}, Ni^{2+}, Zn^{2+}, and Fe^{2+} and "B" represents cation having 3+ charges as for example Al^{3+}, Mn^{3+}, Cr^{3+}, and Fe^{3+}. These two A^{2+} and B^{3+} cations placed either at the octahedral sites or

at the tetrahedral sites depending on their affinity of specific environment. Cation distribution normally depends on the preparation method and their chemical composition [18].

Many research groups have worked on the effect of doping with different cations to see the changes of physical and chemical properties of spinel ferrites such as electrical properties and cationic distribution [19, 20]. Cu^{2+} doped with Fe_3O_4 has attracted much attention towards research due to its wide applications in catalysts, sensors, and electronics and need to develop in each era by using different chemical method or chemical compositions [21]. After knowing the importance of copper ferrite, we report the $Cu_xFe_{1-x}Fe_2O_4$ (where $x = 0$, 0.2, 0.4, 0.6, 0.8 and 1) nanoparticles, synthesized by polyol method and their electrical, chemical and structural properties were discussed in this paper.

2 Experimental

2.1 Chemicals and Instrumentations

$FeCl_3 \cdot 6H_2O$, $FeCl_2 \cdot 4H_2O$, $CuCl_2 \cdot 4H_2O$, diethylene glycol (DEG), and NaOH were taken from Merck and used without further purification.

The crystalline structure of resultant nanoparticles was determined with X-ray diffraction (XRD) measurements using Rigaku D/Max—IIIC with Cu–K_α radiation in the 2θ range of 20–70°.

Fourier transform infrared (FT-IR) spectra were recorded in transmission mode 4000–400 cm^{-1} with a PerkinElmer BX FT-IR infrared spectrometer. The powder samples were ground with KBr and compressed into a pellet.

The surface morphology of the composites was analyzed by scanning electron microscopy (SEM) with JEOL JSM 7001F.

The real (ε') and imaginary (ε'') parts of complex dielectric permittivity $\varepsilon^* \left[= \varepsilon'(\omega) + i\varepsilon''(\omega)\right]$ were measured with a Novocontrol dielectric-impedance analyzer. The dielectric data (ε', ε'') were collected during heating as a function of frequency. The films were sandwiched between gold blocking electrodes and the conductivities were measured in the frequency range 0.1 Hz to 1 MHz at 10 °C intervals. The temperature was controlled with a Novocontrol cryosystem which is applicable between −100 and 250 °C.

2.2 Procedure

DEG-stabilized $Cu_xFe_{1-x}Fe_2O_4$ nanoparticles (NPs) ($x = 0.0$, 0.2, 0.4, 0.6, 0.8, and 1.0) nanoparticles were synthesized by polyol method. Stoichiometric amount of metal salts ($FeCl_2 \cdot 4H_2O$, $FeCl_3 \cdot 6H_2O$, and $CuCl_2 \cdot 4H_2O$) were dissolved in 20 ml of diethylene glycol in three-neck bottom flask using magnetic stirring then 2 M NaOH solution was added drop by drop under constant stirring so that the pH of the solution reached to 11 at which the precipitation of ferrites normally takes place. Then the flask was transferred to the heating mantle apparatus where it was refluxed under the argon condition at the temperature of 180 °C for 3 h. Then NPs were separated by a magnet and washed with distilled water three times. Finally, a dark brown powder product was dried at 80 °C for 4 h.

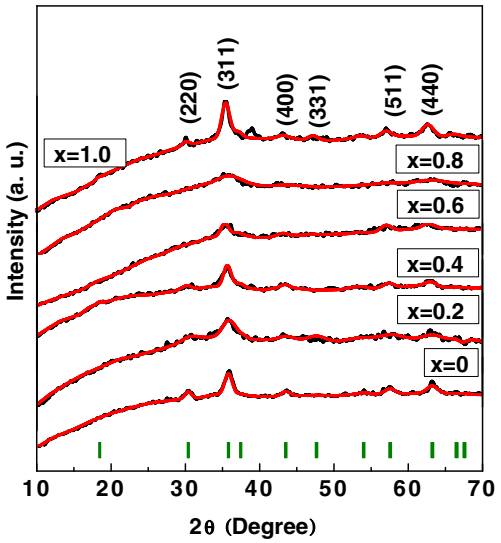

Fig. 1 XRD spectra with Rietveld analysis patterns for DEG-stabilized $Cu_xFe_{1-x}Fe_2O_4$ NPs ($0 \leq x \leq 1.0$)

3 Results and Discussion

3.1 XRD Analysis

XRD data and refinement analyses for DEG-stabilized $Cu_xFe_{1-x}Fe_2O_4$ NPs are shown in Fig. 1. The results of the refinement demonstrated that the main phase in all samples was consistent with the standard pattern for cubic Fe_3O_4

Table 1 Average crystallite sizes of DEG-stabilized $Cu_xFe_{1-x}Fe_2O_4$ nanoparticles estimated by the Debye–Scherrer approximation

x	Crystallite size (nm)
0.0	9.9
0.2	7.8
0.4	8.5
0.6	6.7
0.8	7.4
1.0	10.3

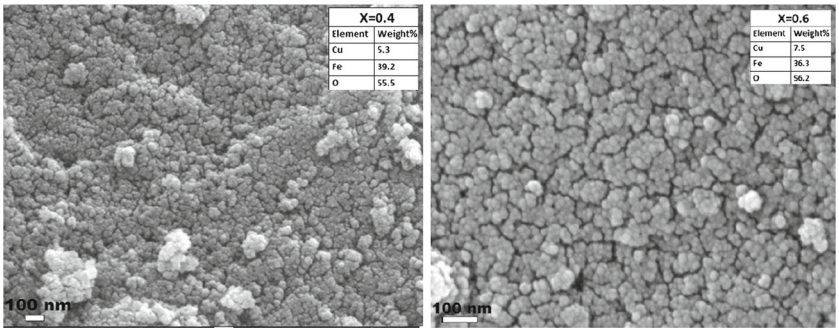

Fig. 2 SEM micrographs of DEG-stabilized $Cu_xFe_{1-x}Fe_2O_4$ NPs for $x = 0.4$ and 0.6

(ICDD card no. 19-629) and $CuFe_2O_4$ (77-0010) respectively with no discernable impurities. The patterns and corresponding Bragg reflections in green bars are depicted and calculated in FullProf program with the space group Fd-3m. The peaks having the following hkl values (220), (311), (400), (331), (511) and (440) confirm the formation of good crystallization with single phase of spinel structure of magnetite and $CuFe_2O_4$ (for $x = 1.0$). The Debye–Scherrer equation was used for the calculation of the crystallite sizes based on 3 1 1 XRD peak for all products and presented in Table 1.

3.2 SEM and EDX Analysis

The SEM micrographs and EDX spectra of the DEG-stabilized $Cu_{0.4}Fe_{1.6}Fe_2O_4$ and $Cu_{0.6}Fe_{1.4}Fe_2O_4$ NPs are presented in Fig. 2. Figure 2 reveals that both compositions have approximately spherical-shaped nanoparticles. The average particle size can be estimated as 10 nm which is less bigger than the crystallite size obtained from XRD powder pattern due to the effect of the relatively stronger interaction between the magnetic particles [22]. EDX spectra (Fig. 2) revealed that the obtained products were composed of the target materials.

3.3 FT-IR Analysis

Figure 3 shows the FT-IR spectra of DEG-stabilized $Cu_xFe_{1-x}Fe_2O_4$ NPs ($0.0 \leq x \leq 1.0$) and pure DEG, respectively. From Fig. 3a, it is seen that the spectrum of pure DEG shows many characteristic peaks like the peaks 1000–1045 and 3400–3465 cm^{-1} which indicate the presence of –C–O and –OH group vibration modes respectively. In Fig. 3, 1465 cm^{-1} band refers to the stretching vibration of C–C of PEG [23–26]. Bands between 2880–1600 and 1195–600 cm^{-1} correspond to the straight deformation of C–H group bending and stretching vibrations, respectively. Figure 3b shows that two characteristic absorption bands from $Cu_xFe_{1-x}Fe_2O_4$ nanoparticles appear at 572 and 628 cm^{-1} due to M–O stretching [27, 28].

3.4 TG Analysis

The presence and proportion of organic compounds (DEG) onto the $Cu_xFe_{1-x}Fe_2O_4$ nanoparticle's surfaces were

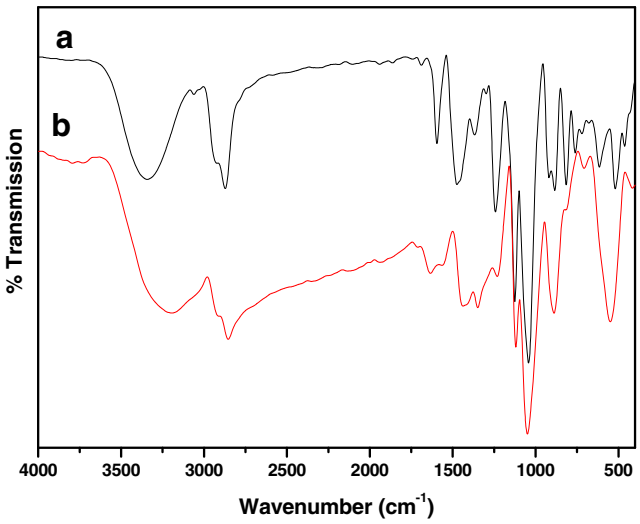

Fig. 3 FT-IR spectra of *a* DEG and *b* DEG-stabilized $Cu_xFe_{1-x}Fe_2O_4$ NPs (for $x = 0.2$)

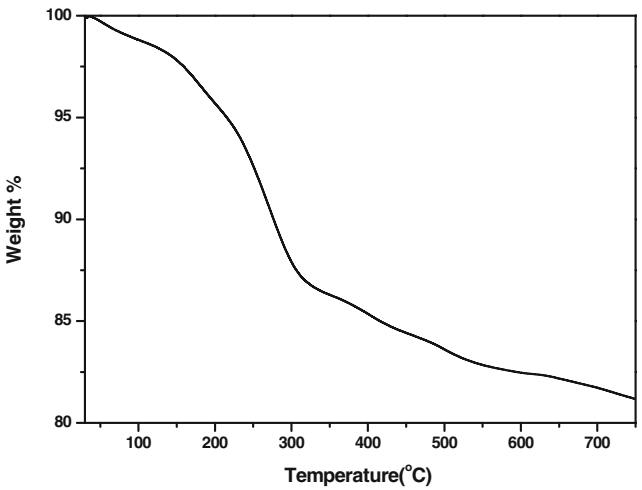

Fig. 4 TGA graph of DEG-stabilized $Cu_xFe_{1-x}Fe_2O_4$ NPs

characterized by using TGA operating between the temperature range of 25 and 750 °C. As it is shown in Fig. 4, about 19 % of the weight of DEG-stabilized $Cu_xFe_{1-x}Fe_2O_4$ NPs was lost in this temperature range. Weight loss slowly started at 50 °C and continued up to 150 °C due to the evaporation of adsorbed water content. Then evaporation of organic content began till 650 °C. This suggests that around 19 % (wt) of the DEG-stabilized $Cu_xFe_{1-x}Fe_2O_4$ NPs was composed of organic compounds (adsorbed water and DEG) and 81 % of it consists of inorganic phase ($Cu_xFe_{1-x}Fe_2O_4$)

3.5 Electrical Properties

3.5.1 AC Conductivity

The ac conductivities, σ_{ac} (ω), of DEG-stabilized $Cu_xFe_{1-x}Fe_2O_4$ NPs with variation of temperature and frequency for different x values are shown in Fig. 5a–f. The frequency-dependent σ_{ac} (ω) were derived using the relation (1)

$$\sigma'(\omega) = \sigma_{ac}(\omega) = \varepsilon''(\omega)\omega\varepsilon_0 \tag{1}$$

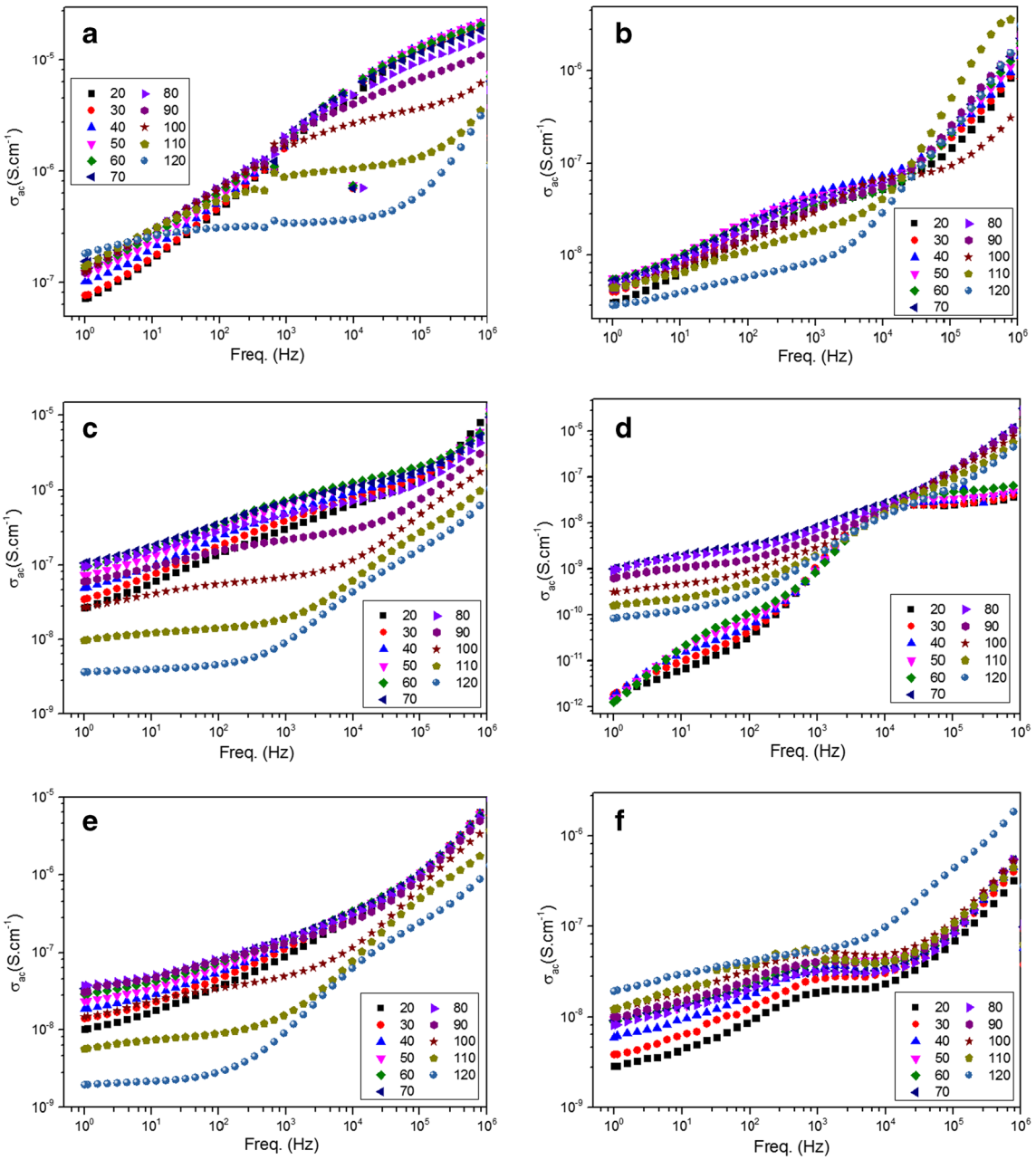

Fig. 5 The variation of ac conductivity of DEG-stabilized $Cu_xFe_{3-x}O_4$ NPs as a function of frequency and temperature for **a** $x = 0$, **b** $x = 0.2$, **c** $x = 0.4$, **d** $x = 0.6$, **e** $x = 0.8$, and **f** $x = 1$

where σ' (ω) is the real part of conductivity, ω ($= 2\pi$) is the angular frequency, ε'' is the imaginary part of complex dielectric permittivity (ε^{ast}), and $\varepsilon_0 (= 8.852 \times 10^{-14}$ F cm^{-1}) is the vacuum permittivity.

The frequency dependency of σ_{ac} and the curves exhibits a similar behavior for all samples of $Cu_xFe_{1-x}Fe_2O_4$ NPs and at all specific temperatures in the log–log plot. The samples exhibited frequency dependency particularly at lower frequency regions and at low temperatures while it shows a significant temperature-dependent behavior at higher temperatures and at medium frequencies. The σ_{ac} generally increases with frequency until certain frequencies and then keeps on rising with changing increment. At high temperatures, the linear increase at low-frequency zone declines or even disappears for $x = 0$, 0.4, and 0.8. The electrode polarization leads to this linear increase in low frequencies and particularly at low temperatures. As temperature increases, the well-distinguished conductivity plateau regions are observed and shift and broaden towards higher frequencies.

In ferrites, electrical conductivity essentially occurs by hopping of electrons between ions of the similar element having multiple valance states which are located randomly onto crystallographically identical lattice sites. The ferrite includes oxygens with cubic close packed lattice structure where the cations reside at the tetrahedral (A) and at the octahedral sites (B).

The hopping of electrons between A and B sites is relatively low as compared to that of B–B hopping due to the fact that the metal ions on A and B sites separated from each other with longer distance [29]. The electron hopping between A and A sites does not take place as iron(III), Fe^{3+}, ions exist only at A sites while any Fe^{2+} or Cu^{2+} ions occupy B sites [30]. When frequency is applied, the charges begin to hop between the acceptable sites contributing to the electrical conductivity. Accordingly, the conductivity enhances with increase in frequency as conduction takes place owing to electron hopping. On the contrary, the conductivity reduces with frequency when the band conduction mainly contributes to the conductivity. In the present case, it is clear that the conductivity is dominated prominently by electron hopping process and the conductivity positively increases with enhancement in frequency for all samples of $Cu_xFe_{1-x}Fe_2O_4$ NPs. The contribution of frequency-dependent conductivity by electron hopping decreases at higher frequencies for $x = 0.6$ which may be due to the charge stabilization between Cu^{2+} and Fe^{2+}.

Figure 6 displays the changes of ac conductivity of DEG-stabilized $Cu_xFe_{1-x}Fe_2O_4$ NPs with temperature at 1 kHz. The plot exhibits almost no increase or slight improvement at low temperature while the conductivity declines markedly over transition temperature of around 80 °C. This indicates

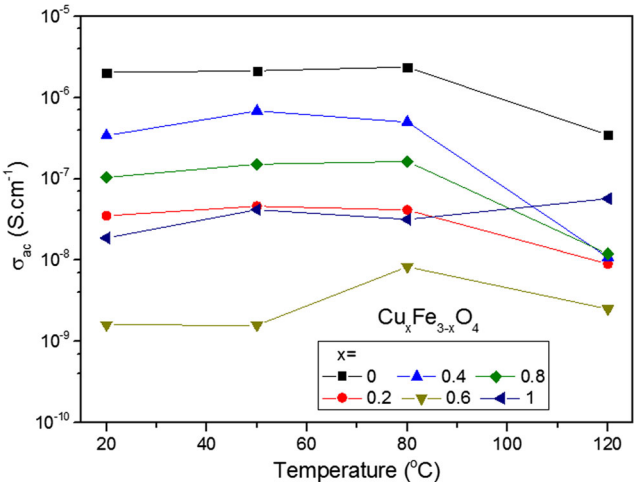

Fig. 6 The variation of ac conductivity of DEG-stabilized $Cu_xFe_{3-x}O_4$ NPs with temperature at 1 kHz

the fact that the temperature dependence of newly synthesized DEG-$Cu_xFe_{1-x}Fe_2O_4$ NPs arises under the specific range of phase transition in NP matrices. The ac conductivity remains nearly constant and shows a maximum near phase transition zone confirming the persistence of reorganization. The reorganization is completed above the transition temperature of 80 °C which is principally resulting from the thermal energy applied on DEG-stabilized $Cu_xFe_{1-x}Fe_2O_4$ NPs [31].

It should be also emphasized that the random distribution of ferrite in nanocomposite is essential for low- and high-frequency response; as a result, a substantial variation in nanocomposite's distribution is observed. Consequently, the conductivity increases regularly with frequency due to the presence of a percolated path within the many nanocomposites, which gives rise to evolution of well-organized plateaus at elevated temperatures. The highest ac conductivity of DEG-stabilized $Cu_xFe_{1-x}Fe_2O_4$ NPs was achieved as 2.4×10^{-6} S cm^{-1} at 80 °C for $x = 0$ since there is no Cu^{2+} that can stabilize charges. The conductivity declines noticeably as temperature increases more (3.5×10^{-7} S cm^{-1} at 120 °C). This fact may be described as the formation of random network at low temperatures, which develops more organized and capacitive behavior at higher temperatures [31, 32].

The DEG-stabilized $Cu_xFe_{1-x}Fe_2O_4$ NPs have lower conductivities than those of pure DEG as compared with previous study [33]. The substitution with Cu^{2+} results in the development of strong electric bonds between the two ions of Cu^{2+} and Fe^{2+} localizing Fe^{2+} charge carriers and hence leading to reduction in electrical conductivity [34]. The lower conductivity, therefore, may be due to the reduction of the free surface charges resulting from surface bonding between DEG and $Cu_xFe_{1-x}Fe_2O_4$ NPs.

3.5.2 DC Conductivity

The dc conductivity (σ_{dc}) versus reciprocal temperature is shown in Fig. 7 for DEG-stabilized $Cu_xFe_{1-x}Fe_2O_4$ NPs. The σ_{dc} was obtained by plotting the graphs of log σ_{ac} versus log freq. by linear fittings. The midpoint was taken for linear fitting to decrease the influence of dispersion and electrode polarization in non-plateau regions.

The dc conductivity curves display the temperature dependency and this behavior might be divided into three specific regions over the temperature range of 20–120 °C. The temperature dependence of conductivity follows the Arrhenius equation

$$\log \sigma_{dc} = \log \sigma_0 - E_a / k_B T \quad (2)$$

where σ_{dc} is the dc conductivity, E_a is the activation energy, σ_0 is the pre-exponential term, k_B is the Boltzmann constant (8.617×10^{-5} eV K^{-1}), and T is the absolute temperature.

It has been shown that the Fe^{2+}–Fe^{3+} interaction and substituted cation ions determine the electrical properties of ferrites [35]. The Verwey de Boer mechanism explained the conduction mechanism of ferrites, which comprises electron exchanges between the ions of the equivalent elements found in several valence states and dispersed over crystallographic lattice sites [36]. The electron exchange might take place between the Fe (II) or Fe (III) ions and Cu^{2+} ions [37]. The increase in charge carrier's drift mobility with temperature leads to improvement in conductivity. The conduction in ferrites is also assigned to electron hopping between Fe^{3+} and Fe^{2+} at higher temperatures [38].

The conductivity plots indicate that conductivity changes with the substitution of Cu^{2+} ions. It is clear that as the ratios of Cu^{2+} ions increase in $Cu_xFe_{1-x}Fe_2O_4$ the conductivity decreases and the lowest conductivity is obtained for $x = 0.2$. The substituted Cu^{2+} ions reside on octahedral sites and it locks up with the iron ions to sustain the charge balance [39]. In octahedral sites, the hopping of electrons between iron ions ($Fe^{2+} \leftrightarrow Fe^{3+}$) decreases by this process and leads to a slight decline in conductivity for all the compositions. As the concentration of Cu^{2+} ions increases (except for $x = 2$), the conductivity decreased considerably which may support that Cu^{2+} ions also normally exist at B sites at higher compositions. The Cu^{2+} ions occupying B sites do not contribute to the conduction because it behaves as scattering centers, and as a consequence, the amount of Fe^{3+} ions reduces [40].

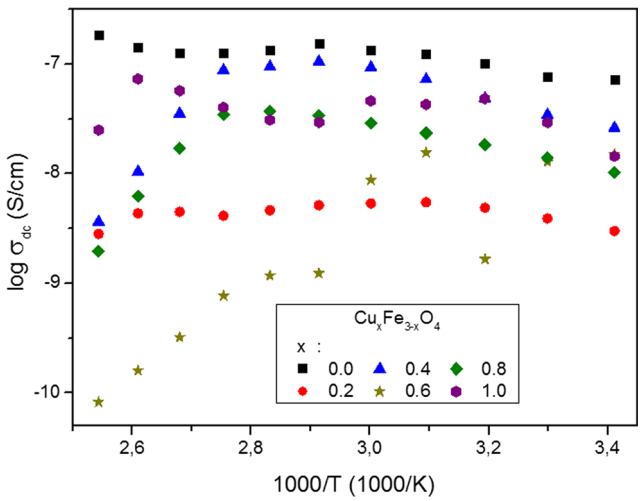

Fig. 7 The variation of dc conductivity of DEG-stabilized $Cu_xFe_{3-x}O_4$ NPs with reciprocal temperature

The significant influence of temperature on dc conductivity is observed between the temperature ranges of 20 and 120 °C under the transition zone around 80 °C. The plot reveals a negative slope at low temperatures and keeps nearly constant at medium temperatures up to a transition temperature of 80 °C. Beyond the transition temperature, another transition occurs and the slope turned out to be positive. These properties exhibit temperature-dependent reorganization of DEG-stabilized $Cu_xFe_{1-x}Fe_2O_4$ NPs under a specific range of phase transition in this structure. The linear increase up to phase transition temperature can be simply explained referring to the number of ions existing in the two sublattices and their corresponding interactions. The Fe^{2+}(A)–$O^{2-}$$Fe^{2+}$(B)-type AB interaction decreases due to the exchange of Fe^{2+} ions with Cu^{2+} ions at the octahedral site. The reduction in Fe^{2+}(A)–$O^{2-}$$Fe^{2+}$(B) interaction leads to a change in transition temperature.

It was shown that the band gap of pure $CuFe_2O_4$ is higher than that of pure Fe_3O_4 [41, 42]. The doping of Cu^{2+} into DEG-stabilized $Cu_xFe_{1-x}Fe_2O_4$ NPs increases the band gap of the NPs and consequently leads to a decrease in conductivity. But the conductivity of the DEG-stabilized $Cu_xFe_{1-x}Fe_2O_4$ NPs does not show the same behavior. It may suggest that both change in amount of defects and band gap resulting in structural deviation, i.e., phase transition, contribute to the conductivity. The structural deviation may be assigned to the stronger or weaker interaction between the second nearest neighbor Fe–O bonds due to the difference in Fe–O bond polarity [43].

The DEG-stabilized $Cu_xFe_{1-x}Fe_2O_4$ NPs reveals change in activation energies with slope before and after transition zone. Here, the conductive activation energy applied at higher temperatures is correlated to the long-distance diffusion of charge carriers; however, the relaxation activation energy associated with the short-distance jumps of charge carrier and it is measured at lower temperatures [44]. With increasing temperature, a sudden decline is observed in σ_{dc} for $x = 0.4$, 0.6, and 0.8 which

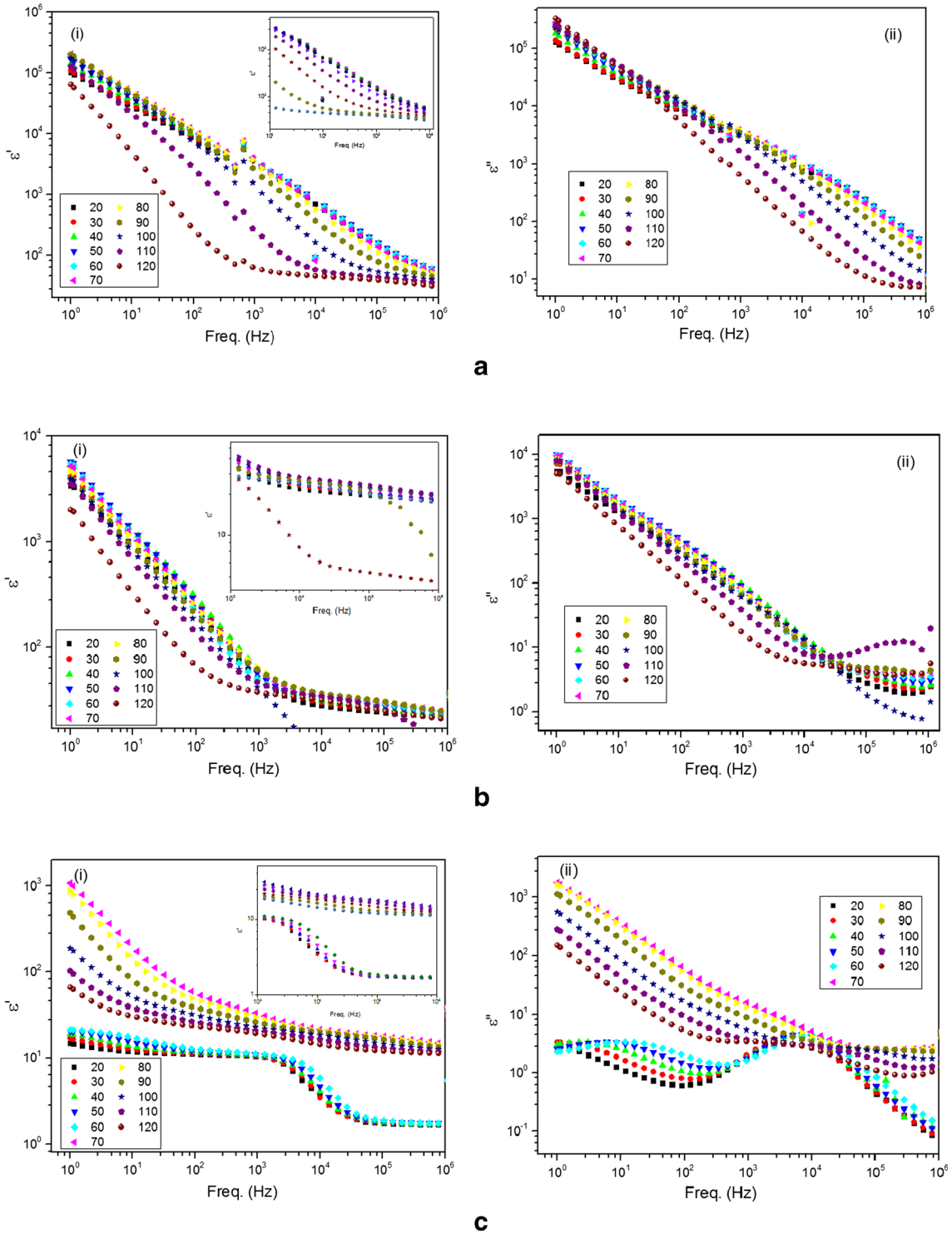

Fig. 8 *i* Real ε' (ε' at high-frequency region *inset*) and *ii* imaginary ε'' parts of permittivity of DEG-stabilized $Cu_xFe_{3-x}O_4$ NPs as a function of frequency at various temperatures for **a** $x = 0.0$, **b** $x = 0.2$, **c** $x = 0.4$, **d** $x = 0.6$, **e** $x = 0.8$, and **f** $x = 1.0$

may show long-distance diffusion conduction mechanism is more effective at elevated temperatures for this NPs. In general, the concentration of cation vacancies increases with introduction of additives, hence accelerates diffusion and enables the phase transition [45]. However, the opposite behavior was observed for $x = 0.4$, 0.6, and 0.8 which may indicate the influence of another parameter on conductivity. The grain size has a substantial effect on the electrical transport properties of NPs. The influence of this grain boundary and grain size on the electrical conductivity of NPs differs

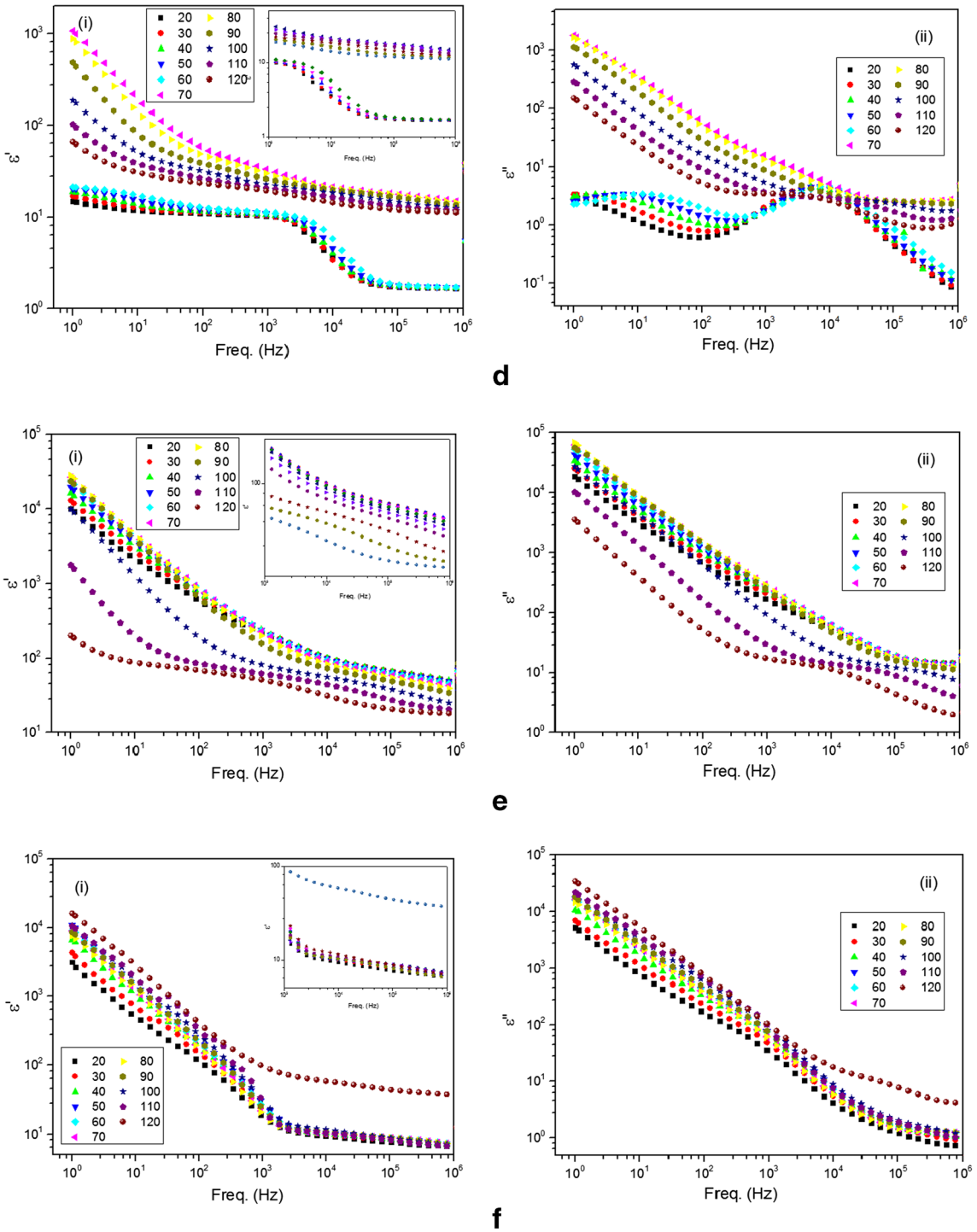

Fig. 8 (continued)

with crystals and temperature range studied [46–48]. In the present study, we observed that grain size is more effective at lower temperatures exhibiting improved conductivities. On the contrary, the influence of grain boundaries increases at higher temperatures leading to a sharp reduction in total conductivity for $x = 0.4$, 0.6, and 0.8 NPs.

3.5.3 Frequency and Temperature Dependence of Dielectric Properties

The change of the dielectric constant (ε') and dielectric loss (ε'') with frequency is studied in the temperature range of 20–120 °C and related curves are displayed in Fig. 8a–f.

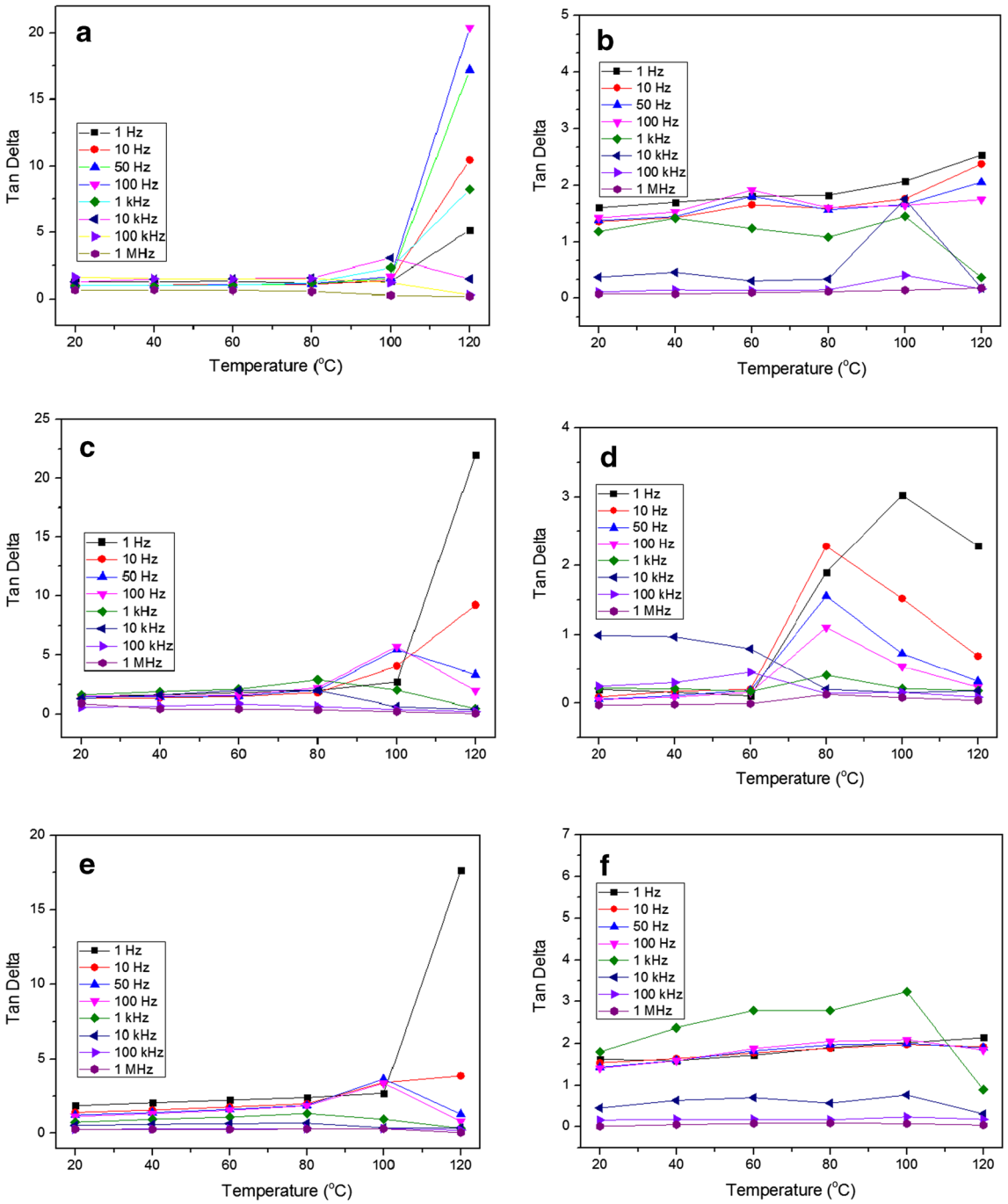

Fig. 9 The tan δ (dissipation factor) variation of DEG-stabilized $Cu_xFe_{3-x}O_4$ NPs as a function of frequency and temperature for **a** $x = 0$, **b** $x = 0.2$, **c** $x = 0.4$, **d** $x = 0.6$, **e** $x = 0.8$, and **f** $x = 1.0$

The ε' of the DEG-stabilized $Cu_xFe_{1-x}Fe_2O_4$ NPs, in general, displays a sharp exponential decline with frequency up to about 1 kHz at low temperatures; however, there is a reduction in ε' which is relatively low at higher temperatures. The rate of decrease in the ε' is quite small over 1 kHz for all samples and shows a curvature at low temperature (<60 °C) shifting slightly to higher frequencies which assigns to the reorganization of NPs at elevated temperatures and phase transition. The ε' remains nearly constant for all x values when $>10^5$ Hz indicating that frequency does not have any effect on the electron exchange between Fe^{2+} and Cu^{2+} over a specific frequency of applied ac field. In general, a considerable decrease is observed in ε' with increasing frequency because dipole

orientations require a longer time than ionic and electronic polarizations, which were also observed for DEG-stabilized $Cu_xFe_{1-x}Fe_2O_4$NPs [49, 50].

The frequency dependence of dielectric constant can be described by the Maxwell–Wagner heterogeneous double-layer structure [51, 52]. The two layers include rather conducting grains separated by the second layer of grain boundaries with poor conductivity [54, 55]. The contribution of grain boundaries is higher at low frequencies while the ferrite grains are more effective at high frequencies [53]. The differences in the resistivity of grains and grain boundaries lead to accumulation of charge carriers in separated boundaries and an improvement in dielectric constants.

The remarkable increase of ε' up to the temperature of 60–70 °C is due to the development of interfaces between $Cu_xFe_{1-x}Fe_2O_4$ NPs and DEG molecules, which is considerably in good agreement with other spinel ferrite [54]. At higher temperatures, ε' either remains almost constant or reduces due to the rubber-like behavior of chemically bonded DEG-stabilized $Cu_xFe_{1-x}Fe_2O_4$ NPs as described for DEG-stabilized $Mn_xCo_{1-x}Fe_2O_4$ NPs. The formation of percolated path facilitates the conduction for this rubber-like NPs [51, 52]. Thus, the ε' of NPs increases prominently until the temperature of 60–70 °C, and subsequently, it declines at higher temperatures. Additionally, the increase in thermal energy results in a significant enhancement in charge carrier's mobility.

The variation of the dielectric loss constant, ε'', with frequency at different temperatures is given in Fig. 8a–f. Generally, a sharp linear decrease is observed with frequency particularly at elevated temperatures. This linearity relates to the σ_{dc} defined by the equation $\varepsilon''_{dc} = \sigma_{dc}(\omega_o)$, where σ_{dc} is the dc conductance and C_o is the vacuum capacitance of empty cell [53]. This behavior may also confirm the dependency of conduction mechanism on both nature of the reorganization and temperature. It is observed that the capacitive response of the DEG-stabilized $Cu_xFe_{1-x}Fe_2O_4$ NPs is rather temperature dependent. Furthermore, the relaxation of conductivity is prominent over other dielectric relaxations under the given temperature and frequency; therefore, $\varepsilon'_{conduct} >> \varepsilon''_{relax}$ [52].

In the region of grain boundaries, polarization needs more energy at lower frequencies which resulted in high-energy loss since the influence of grain boundaries is greater at lower frequencies; however, grains dominate at higher frequencies. On the contrary, it requires less energy for the polarization in the grain region which results in a small energy loss at high frequencies [35, 53]. Electronic and ionic belong to the polarization mechanisms which exist at higher frequencies whereas the interface polarization is significant at lower frequencies [54–56]. Accordingly, at higher frequencies (>10 kHz), dielectric loss constant is less sensitive to both temperature and frequency.

*3.5.4 Dissipation Factor (*tan *δ)*

The dissipation factor (loss tangent, tanδ) ofDEG-stabilized $Cu_xFe_{1-x}Fe_2O_4$ NPs with variation of frequency at different temperatures is shown in Fig. 9a–f. The loss tangent, in general, does not exhibit a remarkable change until 100 °C while a substantial increase was observed at higher temperatures. The temperature dependency of the dielectric loss tangent is described by the polarization mechanism. The electrical conductivity grows with temperature because of the thermal energy and diffusion of the charge carriers. Therefore, the dielectric constant and dielectric loss tangent enhance with increase in dielectric polarization. For pure DEG, the peak maximums of loss tangent can be entirely identified at lower frequencies (<100 Hz) [33]. The disappearance of corresponding peak maximums of loss tangent is possibly due to the development of DEG layer on the surface of $Cu_xFe_{1-x}Fe_2O_4$ NPs which precludes relaxation as a consequence; it may also describe having such low conductivities as compared with a previously similar study [52].

4 Conclusion

The glycol-thermal technique was employed to synthesize DEG-stabilized $Cu_xFe_{1-x}Fe_{2-x}O_4$ NPs at the low reaction temperature of 180 °C. The average crystallite diameter of the products are in the range of 6.97 to 10.3 nm. The σ_{ac} measurements essentially indicated a temperature- and frequency-dependent behavior. The frequency-dependent behavior of σ_{ac} in the low-frequency region mainly rises from the electrode polarization while the temperature dependency is basically due to the hopping process. The σ_{dc} depends on both the concentration of Cu^{2+} ions substituted and temperature. The highest σ_{dc} value was found to be 1.85×10^{-7} S cm^{-1} for $x = 0.0$ at 120 °C. The DEG-stabilized $Cu_xFe_{1-x}Fe_2O_4$ NPs exhibited relatively high dielectric permittivity (between 10^2 and 10^5). The dielectric constants, in general, increase with temperature up to the transition region and thereafter they decrease sharply at higher temperatures. The dielectric measurements suggest that the conduction mechanism depends both on temperature and on the nature of the reorganization of the nanocomposite. Consequently, the observed properties of DEG-stabilized $Cu_xFe_{1-x}Fe_2O_4$ NPs may indicate diverse biomedical applications such as a very promising drug carrier and bioseparator and metal ion separation from waste water.

Acknowledgments This work was supported by Fatih University under BAP Grant No. P50021301-Y (3146). Md. Amir also thanks the Turkish Research Council for his master studies and foreign student's scholarship program of 2215.

References

1. Wang, J., Wu, Y.J., Zhu, Y.J.: Fabrication of complex of Fe_3O_4 nanorods by magnetic-field-assisted solvothermal process. Mater. Chem. Phys. **106**, 1–4 (2007)
2. Zou, G.F., Xiong, K., Jiang, C.G., Li, H., Li, T.W., Du, J., Qian, Y.T.: Fe_3O_4 nanocrystals with novel fractal. J. Phys. Chem. B **109**, 18356–18360 (2005)
3. Hayakawa, H., Tanaka, H., Fujimoto, K.: Preparation of a new precipitated iron catalyst for Fischer–Tropsch synthesis. Catal. Commun. **8**, 1820–1824 (2007)
4. Durmus, Z., Kavas, H., Toprak, M.S., Baykal, A., Altıncekic, T.G., Aslan, A., Bozkurt, A., Cosgun, S.: L-lysine coated iron oxide nanoparticles: synthesis, structural and conductivity characterization. J. Alloys Compd. **484**, 371–376 (2009)
5. Jiang, J., Gu, H., Shao, H., Devlin, E., Papaefthymiou, G.C., Ying, J.Y.: Bifunctional Fe_3O_4-Ag heterodimer nanoparticles for two-photon fluorescence imaging and magnetic manipulation. Adv. Mater. **20**, 4403–4407 (2008)
6. Lin, F.H., Chen, W., Liao, Y.H., Doong, R.A., Li, Y.D.: Effective approach for the synthesis of monodisperse magnetic nanocrystals and M-Fe_3O_4 (M = Ag, Au, Pt, Pd) heterostructures. Nano Res. **4**, 1223–1232 (2011)
7. Schalowa, T., Brandta, B., Starra, D.E., Laurina, M., Schauermanna, S., Shaikhutdinova, S.K., Libuda, J., Freund, H.J.: Oxygen-induced restructuring of a Pd/Fe_3O_4 model catalyst. Catal. Lett. **107**, 189–195 (2006)
8. Hsu, J.H., Chen, S.Y., Chang, W.M., Jian, T.S., Chang, C.R.: Magnetoresistance effect in $AgFe_3O_4$ and Al-Fe_3O_4 composite films. J. Appl. Phys. **93**, 7702–7704 (2003)
9. Yu, C.M., Guo, J.W., Gu, H.Y.: Surface of Au@Fe_3O_4 magnetic nanoparticles. Microchim. Acta **166**, 215–220 (2009)
10. Li, Z.B., Deng, Y.D., Shen, B., Hu, W.B.: Preparation and microwave absorption properties of Ni–Fe_3O_4 hollow spheres. Mater. Sci. Eng. B **164**, 112–115 (2009)
11. Kittel, C.: Nuclear induction. Phys. Rev. **70**, 965–970 (1946)
12. Chundnovsky, E.M., Gunther, L.: Quantum Tunneling of magnetization in small ferromagnetic particles. Phys. Rev. Lett. **60**, 661–667 (1988)
13. Gunther, L.: Quantum tunneling of magnetization. Phys. World **3**(12), 28 (1990)
14. Ziolo, R.F.: US Patent **4**, 474866 (1984)
15. Rosenweig, R.E.: Ferrohydrodynamics. MIT Press, Cambridge (1985)
16. Soibam, I., Phanjoubam, S., Sharma, H.B., Sharma, H.N.K., Laishram, R., Prakash, C.: Effects of cobalt substitution on the dielectric properties of Li–Zn ferrites. Solid State Commun. **148**, 399–402 (2008)
17. Mazen, S.A., Mansour, S.F., Dhahri, E., Zaki, H.M., Elmosalami, T.A.: The infrared absorption and dielectric properties of Li–Ga ferrite. J. Alloy Compd. **470**, 294–300 (2009)
18. Salah, L.M., Moustafa, A.M., Ahmed Farag, I.S.: Structural characteristics and electrical properties of copper doped manganese ferrite. Ceram. Intern. **38**, 5605–5611 (2012)
19. Kumar, S., Kumar, R., Thakur, P., Chae, K.H., Sharma, S.K., Alimuddin: Electronic structure studies of $Mg_{0.95}Mn_{0.05}Fe_{2-2x}Ti_{2x}O_4$ ($0 \leqslant x \leqslant 0.8$). J. Magn. Magn. Mater. **320**, e121–e124 (2008)
20. Gautam, S., Muthurani, S., Balaji, M., Thakur, P., Padiyan, D., Pathinettam, K.H., Chae, S.S., Kim, S.S.A.: Asokan, Electronic structure studies of nanoferrite $Cu_xCo_{1-x}Fe_2O_4$ by X-ray absorption spectroscopy. J. Nanotechnol. **11**, 386–390 (2011)
21. Shin, H.C., Choi, S.C., Jung, K.D., Han, S.H.: Mechanism of M ferrites (M = Cu and Ni) in the CO_2 decomposition reaction. Chem. Mater. **13**, 1238–1242 (2001)
22. Amir, Md., Sertkol, M., Baykal, A., Sözeri, H.: Magnetic and catalytic properties of $Cu_xFe_{1-x}Fe_2O_4$ nanoparticles. J. Supercond. Nov. Magn. (2015)
23. Ahmeda, M.A., Okasha, N., Mansour, S.F., El-dek, S.I.: Bi-modal improvement of the physico-chemical characteristics of PEG and MFe_2O_4 subnanoferrite. J. Alloy. Compd. **496**, 345–350 (2010)
24. Raman, M.S., Kesavan, M., Senthilkumar, K., Ponnuswamy, V.: Ultrasonic, DFT and FT-IR studies on hydrogen bonding interactions in aqueous solutions of diethylene glycol. J. Mol. Liqd. **202**, 115–124 (2015)
25. Sozeri, H., Durmus, Z., Baykal, A.: Structural and magnetic properties of triethylene glycol stabilized $ZnxCo_{1-x}Fe_2O_4$ nanoparticles. Mater. Res. Bull. **47**(9), 2442–2448 (2012)
26. Kazan, S.: Magnetic properties of triethylene glycol coated $CoFe_2O_4$ and $Mn_{0.2}Co_{0.8}Fe_2O_4$ NP's synthesized by polyol method (2012). doi:10.1016/j.arabjc.2011.12.005
27. Deligöz, H., Baykal, A., Tanrıverdi, E.E., Durmus, Z., Toprak, M.S.: Synthesis, structural and electrical properties of triethylene glycol (TREG) stabilized $Mn_{0.2}Co_{0.8}Fe_2O_4$ NPs. Mater. Res. Bull. **47**(3), 537–543 (2012)
28. Günay, M., Erdemi, H., Baykal, A., Sözeri, H., Toprak, M.S.: Triethylene glycol stabilized $MnFe_2O_4$ nanoparticle: synthesis, magnetic and electrical characterization. Mater. Res. Bull. **48**(3), 1057–1064 (2013)
29. Farea, A.M.M., Kumar, S., Batoo, K.M., Yousef, A., Lee, C.G., Alimuddin: Structure and electrical properties of $Co_{0.5}CdxFe_{2.5-x}O_4$ ferrites. J. Alloy. Compd. **464**, 361–369 (2008)
30. Lakshman, A., Subba Rao, P.S.V., Parvatheeswara Rao, B., Rao, K.H.: Electrical properties of In^{3+} and Cr^{3+} substituted magnesium–manganese ferrites. J. Phys. D: Appl. Phys. **38**, 673–678 (2005)
31. Karaoğlu, E., Baykal, A., Erdemi, H., Alpsoy, L., Sözeri, H.: Synthesis and characterization of dl-thioctic acid (DLTA)–Fe_3O_4 nanocomposite. J. Alloys Compd. **509**, 9218–9225 (2011)
32. Lupeiko, T.G., Lopatina, I.B., Kozyrev, I.V., Derbaremdiker, L.A.: Electrophysical and magnetoelectric properties of ceramic materials of the type piezoelectric-ferrite. Inorg. Mater. **28**, 481–485 (1992)
33. Deligöz, H., Baykal, A., Tanrıverdi, E.E., Durmus, Z., Sozeri, H., Toprak, M.S.: Synthesis, structural and electrical properties of triethylene glycol (TREG) stabilized $Mn_{0.2}Co_{0.8}Fe_2O_4$ NPs. Mater. Res. Bull. **47**, 537–543 (2012)
34. Ghodake, J.S., Kambale, R.C., Salvi, S.V., Sawant, S.R., Suryavanshi, S.S.: Electric properties of Co substituted Ni–Zn ferrites. J. Alloy Compd. **486**, 830–834 (2009)
35. Mahalakshmi, S., Srinivasa Manja, K.: AC electrical conductivity and dielectric behavior of nanophase nickel ferrites. J. Alloys Compd. **457**, 522–525 (2008)
36. Verwey, E.J., de Boer, J.H.: Rec. Trans. Chim. Phys. Bas. **55**, 531 (1936)
37. Parvatheeswara Rao, B., Rao, K.H., Sankaranarayana, G., Padurarua, A., Caltun, O.F.: J. Opto. Adv. Mater. **7**, 697–700 (2005)
38. Pardavi-Horvath, M.: Microwave applications of soft ferrites. J. Magn. Magn. Mater. **215–216**, 171–183 (2000)
39. Lakshman, A., Subba Rao, P.S.V., Parvatheeswara Rao, B., Rao, K.H.: J. Phys. D: Appl. Phys. **38**, 673–678 (2005)
40. Lakshman, A., Rao, K.H., Mendiratta, R.G.: J. Magn. Magn. Mater. **250**, 92–97 (2002)
41. Baykal, A., Güner, S., Demir, A.: Synthesis and magneto-optical properties of triethylene glycol stabilized $Mn_{1-x}Zn_xFe_2O_4$ nanoparticles. J. Alloy Compd. **619**, 5–11 (2015)
42. Lemine, O.M., Bououdina, M., Sajieddine, M., Al-Saie, A.M., Shafi, M., Khatab, A., Al-hilali, M., Henini, M.: Synthesis, structural, magnetic and optical properties of nanocrystalline $ZnFe_2O_4$. Physica B **406**, 1989–1994 (2011)

43. Kaushal, A., Pathak, D., Bedi, R.K., Kaur, D.: Structural, electrical and optical properties of transparent $Zn_{1-x}Mg_xO$ nanocomposite thin films. Thin Solid Films **518**, 1394–1398 (2009)
44. Li, D., Wang, X.P., Fang, Q.F., Wang, J.X., Li, C., Zhuang, Z.: Phase transition associated with the variation of oxygen vacancy/ion distribution in the oxide-ion conductor $La_2Mo_{2-x}W_xO_9$. Physica Status Solidi A **7**, 2270–2278 (2007)
45. Taşçıoğlu, İ., Arı, M., Usluc, İ., Koçyiğit, S., Dağdemir, Y., Çorumlu, V., Altındal, Ş.: Temperature dependent conductivity and structural properties of sol–gel prepared holmium doped Bi_2O_3 nanoceramic powder. Ceram. Int. **38**, 6455–6460 (2012)
46. Kang, Y.J., Park, H.J., Choi, G.M.: The effect of grain size on the low-temperature electrical conductivity of doped CeO_2. Solid State Ionics **179**, 1602–1605 (2008)
47. Djuric, Z.Z., Aleksic, O.S., Nikolic, M.V., Labus, N., Radovanovic, M., Lukovic, M.D.: Structural and electrical properties of sintered Fe_2O_3/TiO_2 nanopowder mixtures. Ceram. Intl. **40**, 15131–15141 (2014)
48. Guo, X.: Peculiar size effect in nanocrystalline $BaTiO_3$. Acta Materialia **61**, 1748–1756 (2013)
49. Iqbal, M.J., Ismail, B.: Correlation between structural and electrical properties of $Mg_{1-2}xZnxNixAl_2O_4$ (x = 0.0–0.5) ceramic nanomaterials synthesized by a urea assisted microwave combustion method. J. Alloy. Compd. **504**, 440–445 (2010)
50. Afandiyeva, İ.M., Dökme, İ., Altındal, Ş., Bülbül, M.M., Tataroğlu, A.: Frequency and voltage effects on the dielectric properties and electrical conductivity of Al–TiW–Pd_2Si/n-Si structures. Microelectr. Eng. **85**, 247–252 (2008)
51. Ünal, B., Durmus, Z., Baykal, A., Sözeri, H., Toprak, M.S., Alpsoy, L.: L-Histidine coated iron oxide nanoparticles: synthesis, structural and conductivity characterization. J. Alloys Compd. **505**, 172–177 (2010)
52. Durmus, Z., Kavas, H., Baykal, A., Sozeri, H., Alpsoy, L., Çelik, S.Ü., Toprak, M.S.: Synthesis and characterization of l-carnosine coated iron oxide nanoparticles. J. Alloys Compd. **509**, 2555–2561 (2011)
53. Manjurul Haquea, M., Huqa, M., Hakim, M.A.: Densification, magnetic and dielectric behaviour of Cu-substituted Mg–Zn ferrites. Mater. Chem. Phys. **112**, 580–586 (2008)
54. Erdemi, H., Demir, A., Baykal, A.: Electrical properties of triethylene glycol stabilized $Mn_x\ Co_{1-x}\ Fe_2\ O_4$ nanoparticles. J. Inorg. Organomet. Polym. **23**, 690–702 (2013)
55. McCrum, N.G., Read, B.E., Williams, G.: Anelastic and Dielectric Effects in Polymeric Solids. Dover Publications, New York (1991)
56. Bozkurt, A.: Dielectric and conductivity relaxations in quaternary ammonium polymer. J. Phys. Chem. Solids **63**, 685–692 (2002)